

# Dalton Transactions

Accepted Manuscript



This is an *Accepted Manuscript*, which has been through the Royal Society of Chemistry peer review process and has been accepted for publication.

*Accepted Manuscripts* are published online shortly after acceptance, before technical editing, formatting and proof reading. Using this free service, authors can make their results available to the community, in citable form, before we publish the edited article. We will replace this *Accepted Manuscript* with the edited and formatted *Advance Article* as soon as it is available.

You can find more information about *Accepted Manuscripts* in the [Information for Authors](#).

Please note that technical editing may introduce minor changes to the text and/or graphics, which may alter content. The journal's standard [Terms & Conditions](#) and the [Ethical guidelines](#) still apply. In no event shall the Royal Society of Chemistry be held responsible for any errors or omissions in this *Accepted Manuscript* or any consequences arising from the use of any information it contains.

## ARTICLE

# Well-controlled Metal Co-catalysts Synthesised by Chemical Vapour Impregnation for Photocatalytic Hydrogen Production and Water Purification

Cite this: DOI:  
10.1039/x0xx00000x

Received 00th January 2012,  
Accepted 00th January 2012

DOI: 10.1039/x0xx00000x

www.rsc.org/

Ren Su,<sup>a</sup> Michael M. Forde,<sup>b,c</sup> Qian He,<sup>d</sup> Yanbin Shen,<sup>a,e</sup> Xueqin Wang,<sup>a,f</sup> Nikolaos Dimitratos,<sup>b,g</sup> Stefan Wendt,<sup>a</sup> Yudong Huang,<sup>f</sup> Bo B. Iversen,<sup>a,e</sup> Christopher J. Kiely,<sup>d</sup> Flemming Besenbacher,<sup>a,\*</sup> and Graham J. Hutchings,<sup>b,g,\*</sup>

**Abstract:** As co-catalyst materials, metal nanoparticles (NPs) play crucial roles in heterogeneous photocatalysis. The photocatalytic performance strongly relies on the physical properties (*i.e.*, composition, microstructure, and surface impurities) of the metal NPs. Here we report a convenient chemical vapour impregnation (CVI) approach for the deposition of monometallic-, alloyed, and core-shell structured metal co-catalysts onto the TiO<sub>2</sub> photocatalyst. The as-synthesised metal NPs are highly dispersed on the support and show narrow size distributions, which suit photocatalysis applications. More importantly, the surface of the as-synthesised metal NPs are free of protecting ligands, enabling the photocatalysts to be ready to use without further treatment. The effect of the metal identity, the alloy chemical composition, and the microstructure on the photocatalytic performance has been investigated for hydrogen production and phenol decomposition. Whilst the photocatalytic H<sub>2</sub> production performance can be greatly enhanced by using the core-shell structured co-catalyst (Pd<sub>shell</sub>-Au<sub>core</sub> and Pt<sub>shell</sub>-Au<sub>core</sub>), the Pt<sub>shell</sub>-Au<sub>core</sub> modified TiO<sub>2</sub> yields enhanced quantum efficiency but a reduced effective decomposition of phenol to CO<sub>2</sub> compared to that of the monometallic counterparts. We consider the CVI approach provides a feasible and elegant process for the decoration of photocatalyst materials.

## Introduction

As a branch of heterogeneous catalysis, semiconductor-based photocatalysis has received great attention over the last decades both in application-oriented and fundamental investigations.<sup>1-3</sup> The photocatalyst materials (*i.e.*, TiO<sub>2</sub>, CdS, ZnO) have shown utilities in photocatalytic water splitting and hydrogen evolution, water and air purifications, destruction of microorganisms, fixation of nitrogen, and clean-up of oil spills.<sup>4-7</sup> However, improving the quantum efficiencies of the materials remains a challenging task to realise large-scale applications of photocatalysis.<sup>8, 9</sup> Engineering the physical properties of the materials has been employed to enhance the photocatalytic performance. The crystallinity, grain size, impurity concentrations, and polymorph composition of the semiconductor photocatalyst materials not only influence the recombination kinetics of the photogenerated electron-hole pairs and related radical species, but could also alter the adsorption/desorption of the reactants on the photocatalyst surface.<sup>10-13</sup>

Surface decoration of the photocatalysts with co-catalyst materials has been considered to be an effective approach to tune the photoreactivity.<sup>14-16</sup> In the photocatalytic hydrogen production process, noble metal (*i.e.*, Au, Pd, Pt) nanoparticles (NPs) as promoters have shown to be essential in achieving

high quantum efficiencies.<sup>17-20</sup> The roles of the metal NPs include trapping the excited electrons and releasing them to the electron acceptor.<sup>21, 22</sup> Therefore optimisation of these two reaction steps is pivotal to enhance the H<sub>2</sub> evolution performance. It has also been demonstrated that metal oxides (*i.e.*, RuO, CoO<sub>x</sub>) and metal sulfides (*i.e.*, PbS<sub>x</sub>, MoS<sub>x</sub>) NPs are excellent promoters for photocatalytic hydrogen and oxygen evolution, and the interplay of the above mentioned composites with metal NPs could even further boost the photocatalytic performance of the semiconductor materials.<sup>23-25</sup>

The surface engineering of photocatalysts has also been investigated in water purification process.<sup>26-28</sup> The presence of metal NPs as co-catalysts has been shown an efficient approach in accelerating the full decomposition of various model organic molecules (*i.e.*, ethanol, acetone) and dye molecules (*e.g.*, methylene blue).<sup>27</sup> Recently, it has been shown that the metal NPs not only serve as electron sinks but are also involved in the photocatalytic decomposition of phenol, and the metal identity influences the stability of the photocatalysts.<sup>29</sup>

Whilst a promotion effect is often observed with the presence of metal NPs co-catalysts, contradictory observations have also been reported, especially in photo-oxidation reactions, indicating the complexity of the function of co-catalysts in photocatalytic reactions.<sup>30, 31</sup> Since the photocatalytic performance is governed by the electronic

properties of the catalyst materials, precise control of the size, chemical composition, and microstructure of the co-catalyst is the key to improve the quantum efficiency of the photocatalyst.<sup>32-34</sup> Conventional sol-gel immobilisation approaches have been employed due to the potential of fine tuning the physical parameters of the metal co-catalysts NPs.<sup>35</sup> However, protecting ligands (*e.g.*, poly vinyl alcohol, PVA) are commonly used during the synthesis of metal colloids, which are subsequently attached to the surface of the as-prepared photocatalysts during the deposition process. The surface ligands may alter (most likely block) the charge transfer dynamics between the photocatalyst and the charge acceptor/donor, as well as the affinity of the reactants to adsorb on the active sites. Post-treatment (*e.g.*, annealing) of the photocatalysts can be employed to remove the surface ligands but the physical parameters of the catalysts (*i.e.*, size, structure, and composition) may change as well.<sup>29, 37</sup> Therefore, an advanced synthesis protocol that provides clean surface and fine control of the metal NPs is largely in demand.

Herein, we present a chemical vapour impregnation (CVI) method for the deposition of clean, well-controlled metal NPs onto photocatalyst materials. Monometallic, bimetallic, and core-shell structured NPs have been deposited on TiO<sub>2</sub> for demonstration. All metal NPs are characterised by similar fine dispersions and very narrow size distributions. Photocatalytic hydrogen evolution and phenol decomposition have been studied to explore the influence of chemical and structural composition of the metal co-catalyst NPs on the performance.

## Experimental section

### Preparation methods

A chemical vapour impregnation (CVI) method has been used for the deposition of monometallic (Pt and Pd), alloy (Pt<sub>1</sub>Pd<sub>1</sub>) and core-shell (Pt<sub>shell</sub>Au<sub>core</sub> (Pt<sub>s</sub>Au<sub>c</sub>) and Pd<sub>shell</sub>Au<sub>core</sub> (Pd<sub>s</sub>Au<sub>c</sub>), co-catalysts.<sup>38</sup> The TiO<sub>2</sub> support was Degussa P25 (S<sub>BET</sub> ≈ 50 m<sup>2</sup>·g<sup>-1</sup>, ~80 % anatase and ~20 % rutile) and the overall metal loading was 2.5 wt% for all samples. For the preparation of monometallic and alloy supported on TiO<sub>2</sub>, desired amount of TiO<sub>2</sub>, palladium acetylacetonate (Pd(acac)<sub>2</sub>, Sigma-Aldrich, >99%) and/or platinum acetylacetonate (Pt(acac)<sub>2</sub>, Sigma-Aldrich, 99.9%) were mixed and transferred to a Schlenk flask and evacuated at room temperature by a vacuum line (P<sub>min</sub> = 10<sup>-3</sup> mbar). Then the mixture was kept at 140 °C for 1 h under vacuum conditions with continuous stirring to achieve the sublimation and deposition of the organometallic precursors onto the support. Subsequently the samples were placed into a quartz boat and heat treated in a 5 % H<sub>2</sub>/Ar atmosphere at 400 °C for 3 h to fully pyrolyse the metal precursors. Due to the scarcity of Au precursors for vapour deposition, the core-shell structured co-catalysts supported on TiO<sub>2</sub> were prepared *via* a hybrid CVI/sol-immobilization (SI) technique in the following manner. Firstly, a 1 wt% of Au supported on TiO<sub>2</sub> was prepared using the SI methodology with water reflux treatment (90 °C, 1h) before drying to remove the PVA ligand shell.<sup>39</sup> Then the required amount of Pd(acac)<sub>2</sub> or Pt(acac)<sub>2</sub> was mixed with the dried and ground, pre-formed Au/TiO<sub>2</sub> and transferred to a Schlenk tube to perform the standard CVI process described above. Details of the preparation can be found in our previous work.<sup>38</sup> Due to the poor stability of Au precursors (*e.g.*, dimethylgold acetylacetonate) under synthesis conditions, the preparation of a 2.5 wt% Au/TiO<sub>2</sub> was realised by a standard photodeposition method. Previous research indicate that the photodeposited Au

NPs are ligand free and show particle size of ~4-5 nm, which is comparable to that of CVI prepared metal NPs.<sup>40</sup>

### Characterisation of physical properties

High-angle annular dark-field (HAADF) imaging of the co-catalyst NPs were taken using a scanning transmission electron microscope (STEM, JEOL 2200FS) equipped with a probe aberration corrector (CEOS). The STEM samples were prepared by dry dispersing the catalyst powder onto a holey carbon TEM grid. The microscope is also equipped with a Thermo-Noran X-ray energy dispersive spectroscopy (XEDS) system. The crystallographic information of the samples was analyzed by X-ray diffraction (XRD) using an X-ray diffractometer (SmartLab, Rigaku) with Cu-K $\alpha$  radiation. The scan rate and integration time were 0.04 deg·s<sup>-1</sup> and 10.0 s, respectively. X-ray Photoelectron Spectroscopy (XPS) were recorded on a Kratos Axis Ultra spectrometer. A monochromatic Al K $\alpha$  source (10 mA, 15 kV) was employed for the analysis. Pass energies of 160 eV and 40 eV were used for survey scans and high resolution scans, respectively. The binding energy scale was referenced to the C1s binding energy of 284.8 eV of adventitious carbon.

### Photo-catalytic performance evaluations

A UV LED (365 nm, Optimax 365) with a photon flux of 4 x 10<sup>17</sup> photons·s<sup>-1</sup> was used in all experiments. The photocatalytic H<sub>2</sub> production and phenol decomposition was carried out in a leak-tight reactor that was connected to a mass spectrometer (MS, Hiden HPR-20). For H<sub>2</sub> evolution, 25 mg of the catalyst was dispersed in 25 ml of 25 vol% ethanol and kept in the dark for 30 min to establish adsorption equilibrium prior to experiment. The reactor was then evacuated for 30 min until the dissolved O<sub>2</sub> reduced to ~5  $\mu$ M. A two-hour irradiation was employed for the H<sub>2</sub> evolution process under continuous stirring and the partial pressures of m/e = 2 (H<sub>2</sub>), 18 (H<sub>2</sub>O), 28 (N<sub>2</sub>), 32 (O<sub>2</sub>), and 44 (CO<sub>2</sub>) were monitored *in-situ*. For phenol decomposition, the evolution of CO<sub>2</sub> was carried out under ambient conditions. The photo-catalysts (1 g·L<sup>-1</sup>) were added into 25 mL phenol solutions (400  $\mu$ M). The suspensions were kept in the dark for 1 h to establish adsorption equilibrium. Deionised (DI) water was used throughout the experiments. Details of the photo-reactivity measurement and related calculations have been reported elsewhere.<sup>29</sup>

The evolved H<sub>2</sub> can be quantified by the following equations:<sup>21</sup>

$$n(\text{H}_2)_{\text{gas}} = p(\text{H}_2)_{\text{rea}} \times V_{\text{rea}} / RT \quad (1)$$

$$p(\text{H}_2)_{\text{rea}} = \text{RSF}(\text{H}_2) \times p(\text{H}_2)_{\text{det}} \times p(\text{Air})_{\text{rea}} / p(\text{Air})_{\text{det}} \quad (2)$$

where,

$p(\text{H}_2)_{\text{rea}}$  is the partial pressure of H<sub>2</sub> in the reaction chamber;

$p(\text{H}_2)_{\text{det}}$  is the partial pressure of H<sub>2</sub> detected by the MS;

$p(\text{Air})_{\text{rea}}$  is the pressure of air in the reactor (100 kPa);

$p(\text{Air})_{\text{det}}$  is the pressure of air detected by the MS;

$V_{\text{rea}}$  is the gas-phase volume of the reactor (190 mL);

RSF(H<sub>2</sub>) is the relative sensitivity factor of H<sub>2</sub> (0.284).

Since CO<sub>2</sub> is soluble in water, the total amount of evolved CO<sub>2</sub> ( $n(\text{CO}_2)_{\text{total}}$ ) from phenol decomposition consists of evolved CO<sub>2</sub> in gas phase ( $n(\text{CO}_2)_{\text{gas}}$ ) and dissolved CO<sub>2</sub> ( $n(\text{CO}_2)_{\text{liquid}}$ ) in liquid phase, and can be determined as the following:

$$n(\text{CO}_2)_{\text{total}} = n(\text{CO}_2)_{\text{gas}} + n(\text{CO}_2)_{\text{liquid}} \quad (3)$$

$$n(\text{CO}_2)_{\text{liquid}} = p(\text{CO}_2)_{\text{rea}} \times V_{\text{liquid}} / k(\text{CO}_2) \quad (4)$$

where,

$V_{\text{liquid}}$  is the liquid volume (25 mL);

$k(\text{CO}_2)$  is the Henry's law constant of  $\text{CO}_2$  at RT ( $29.41 \text{ L}\cdot\text{atm}\cdot\text{mol}^{-1}$ ).

## Results and discussion

### Physical properties of the photocatalysts

We first characterised the size distributions and the microstructure of the metal NPs by HAADF imaging, as shown in Fig. 1 and Fig. S1 in supplementary materials. All metal NPs regardless of the identity have been uniformly deposited on the  $\text{TiO}_2$ , as representatively depicted by the low-magnification HAADF-STEM images of Pd/ $\text{TiO}_2$  (Fig. 1a). The size distributions of the metal NPs determined by statistical analysis of the HAADF-STEM images are demonstrated in Fig. 1(b).<sup>38</sup> All metal NPs showed very narrow size distributions with mean particle sizes below 4 nm. We also noted that the monometallic Pt NPs presented the minimum mean particle size (1.5 nm) whereas the monometallic Pd NPs exhibited a slightly larger mean particle size (2.8 nm).

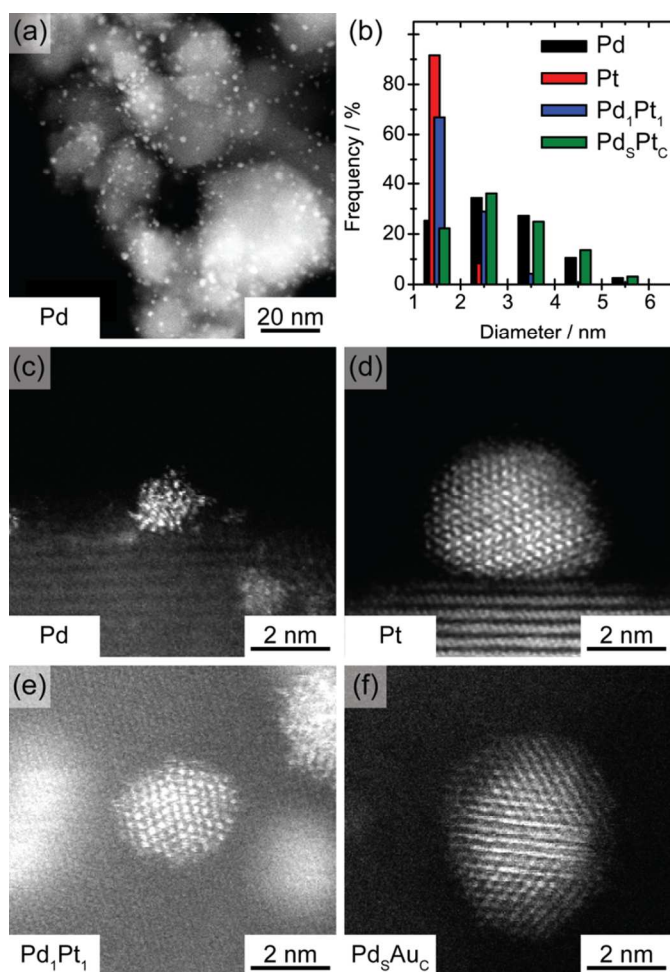


Fig. 1. (a): Representative low-magnification HAADF-STEM image of Pd for the estimation of particle size distribution. (b): Derived particle size distributions of the metal NPs variants.<sup>38</sup> (c)-(f): Representative high-magnification HAADF-STEM images of individual Pd, Pt, Pd<sub>1</sub>Pt<sub>1</sub>, and Pd<sub>5</sub>Au<sub>C</sub> NPs supported on  $\text{TiO}_2$ , respectively.

In comparison with the conventional sol-immobilisation method, the CVI approach provides a solution for the preparation of even smaller metal NPs. Remarkably, the presence of sub-nanometer clusters and isolated atoms was also observed, considering the high-temperature treatment ( $400 \text{ }^\circ\text{C}$ ) during the final preparation (Figure S2 in supplementary materials). This again highlighted the advantage of CVI method for the synthesis of extremely fine dispersion of NPs with high thermal stability, where the sol-immobilised metal NPs suffer extensive particle growth at heat treatment temperature above  $200 \text{ }^\circ\text{C}$ .<sup>29</sup>

We further performed high-magnification HAADF imaging to analyse the morphologies of the individual metal NPs deposited on  $\text{TiO}_2$ , as representatively shown in Fig. 1 (c)-(f). Both monometallic Pd (Fig. 1c) and Pt (Fig. 1d) NPs were attached to the  $\text{TiO}_2$  support and can be characterised by a spherical structure. Whilst the Pd<sub>1</sub>Pt<sub>1</sub> alloy showed a homogeneous distribution of the Pd and Pt atoms (Fig. 1e), a bright core and a dark shell regions were clearly observed for the Pd<sub>5</sub>Au<sub>C</sub> NP (Fig. 1f) due the distinct difference of the atomic number of Au and Pd. It should note that both secondary Pd and uncoated Au NPs were also observed within the Pd<sub>5</sub>Au<sub>C</sub>/ $\text{TiO}_2$  sample.<sup>38</sup>

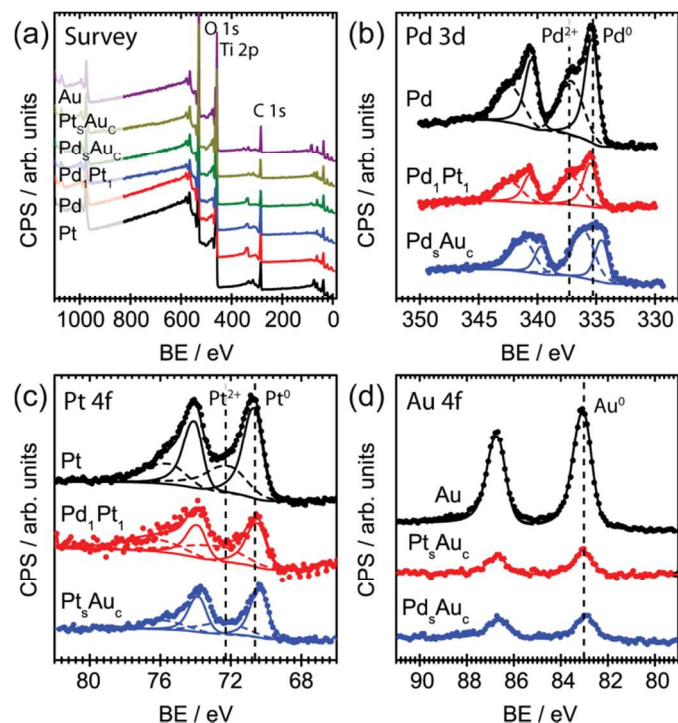


Fig. 2. (a): XPS survey spectra of the as-prepared metal NPs supported on  $\text{TiO}_2$ . (b)-(d): High resolution XPS spectra of Pd 3d, Pt 4f and Au 4f, respectively. The solid and dashed lines are fitting results of the raw data (dots). All catalysts have a total metal loading of 2.5 wt%.

The chemical compositions, as well as the oxidation states of the elements within the as-prepared catalysts were evaluated by XPS, as demonstrated in Fig. 2. The survey spectra (Fig. 2a) suggested that all samples are mainly stoichiometrically  $\text{TiO}_2$  with solely surface adventitious C and small amount of metal species, which indicates that the CVI process has a negligible effect on the  $\text{TiO}_2$  substrate (Fig. S3 in supplementary materials). The high resolution spectra of Pd, Pt, and Au within

related samples were presented in Fig. 2(b)-(d), respectively. A reduced peak intensity of Pd was noticed for both Pd<sub>1</sub>Pt<sub>1</sub> and Pd<sub>5</sub>Au<sub>5</sub> in comparison with monometallic Pd due to the total metal loading was 2.5 wt% in all cases. Both Pd<sup>0</sup> (335.2 eV) and Pd<sup>2+</sup> (337.2 eV) species were observed in all Pd-containing NPs.<sup>41</sup> The Pd<sup>0</sup>: Pd<sup>2+</sup> ratio for the monometallic Pd NPs was ~1:1, and the concentration of Pd<sup>2+</sup> was slightly increased within both Pd<sub>1</sub>Pt<sub>1</sub> and Pd<sub>5</sub>Au<sub>5</sub> due to the interaction with Pt and Au. Besides, a negative shift (~ 0.8 eV) of both peaks was also noticed for the Pd<sub>5</sub>Au<sub>5</sub>. Whilst a similar phenomenon was observed in Pt 4f spectra except that the Pt<sup>0</sup> was the dominant species in all samples (Fig. 3c),<sup>42</sup> the oxidation state of Au remained to be solely metallic in all samples (Fig. 3d).

Additionally, as XPS is a surface sensitive technique, the peak intensity also reflects the microstructure of the material. Note that the intensities of Au 4f peaks reduced significantly in both core-shell NPs (Pd<sub>5</sub>Au<sub>5</sub> and Pt<sub>5</sub>Au<sub>5</sub>). This strongly indicates the presence of the shielding effect that originated from the shell element (Pt or Pd) in addition to the reduced Au loading of these two samples. If we assume that the averaged shell thickness was 1 nm (see Fig. 1f), the reduction of Au 4f peak intensities can be estimated using the Beer-Lambert law and the inelastic mean free path of Pd (18.79 Å) and Pt (15.95 Å).<sup>43</sup> The estimated reduction of the peak intensities was ~41 % and 47 % for the Pd<sub>5</sub>Au<sub>5</sub> and Pt<sub>5</sub>Au<sub>5</sub> NPs, respectively, which agreed well with the observation (42 % and 50 % for Pd<sub>5</sub>Au<sub>5</sub> and Pt<sub>5</sub>Au<sub>5</sub> NPs). Although the calculation was very rough, it suggested that the majority of the Pd<sub>5</sub>Au<sub>5</sub> and Pt<sub>5</sub>Au<sub>5</sub> NPs can be characterised by the core-shell structure.

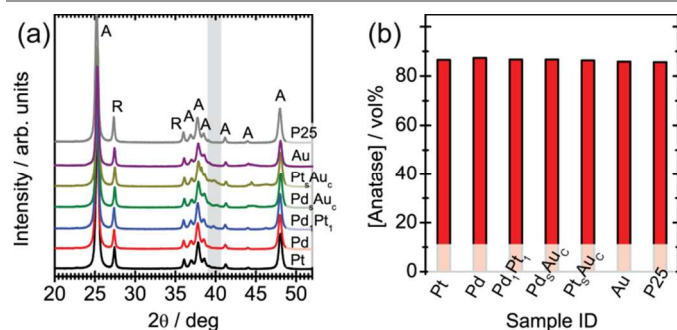


Fig. 3. (a): XRD patterns of the as-prepared metal NPs supported on TiO<sub>2</sub>. Au/TiO<sub>2</sub> prepared by photodeposition<sup>40</sup> and a pristine TiO<sub>2</sub> (P25) are presented for comparison. A and R indicate the peak positions of anatase and rutile, respectively. The gray zone indicates the possible peak positions of the metal NPs. (b): Polymorph compositions of the as-prepared metal NPs supported on TiO<sub>2</sub> derived by XRD patterns.

We further performed X-ray diffraction analysis to examine whether the metal decoration process has an influence on the crystallographic properties of the TiO<sub>2</sub> substrate. The XRD patterns of all catalysts, along with a Au/TiO<sub>2</sub> catalyst prepared by photodeposition<sup>40</sup> and a pristine TiO<sub>2</sub> (P25) for comparison, were shown in Fig. 3(a). It was clear that all materials (both metal decorated and bare TiO<sub>2</sub>) show similar diffraction patterns. The full widths at half maximum (FWHM) of the characteristic peaks of anatase and rutile were identical compared to that of the bare P25, indicating the volume

averaged crystallite size of both polymorphs remained unchanged. The polymorph composition, which was derived from the peak intensities of anatase and rutile,<sup>12</sup> also kept constant after the decoration (Fig. 3b). This information again suggested that the CVI deposition process show a negligible effect on the TiO<sub>2</sub> support. Note very broad and weak peaks that assigned to the fine metals NPs can be observed at 2θ = ~ 40° (gray zone in Fig. 3a), which agreed well with the observation from HAADF-STEM images.

Therefore, we conclude that the as-synthesised metal NPs supported on TiO<sub>2</sub> are characterised by small particle size with narrow size distributions and have exposed clean surfaces for catalytic reactions.

### The influence of co-catalysts on the photocatalytic performance

Figure 4(a) demonstrates the *in situ* measurements of photocatalytic H<sub>2</sub> evolution using all the catalysts. The Au/TiO<sub>2</sub> that was synthesised *via* a standard photo-deposition method was also evaluated for comparison.<sup>40</sup> We have also tested the pristine TiO<sub>2</sub> but no H<sub>2</sub> evolution was observed in this case. It was clear that all the metal NPs supported on TiO<sub>2</sub> catalysts can produce H<sub>2</sub> continuously under UV irradiation, and all catalysts produced by the CVI method exhibited faster H<sub>2</sub> evolution rates than that of the photo-deposited Au NPs. However, the performance varies significantly depending on both composition and structure of the metal NPs. We have further quantified the H<sub>2</sub> production rates and apparent quantum efficiencies (AQE) of all the catalysts, as shown in Fig. 4(b). The AQE was derived using the following equation:

$$\text{AQE} = 2n(\text{H}_2)/n(\text{incident photons}) \quad (5)$$

where  $n(\text{H}_2)$  and  $n(\text{incident photons})$  are the numbers of generated H<sub>2</sub> molecule and incident photons within two hours, respectively.

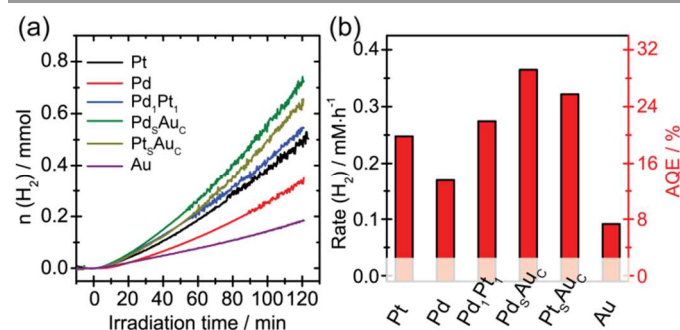


Fig. 4. (a): Photocatalytic H<sub>2</sub> evolution using the as-prepared metal NPs supported on TiO<sub>2</sub> catalyst materials. A 25 vol% of ethanol solution (25 mL) was used for all measurements. (b): The derived H<sub>2</sub> production rates and apparent quantum efficiencies (AQE) of the metal NPs supported on TiO<sub>2</sub> catalyst materials. All catalysts have a metal loading of 2.5 wt%.

Both monometallic Pt and Pd supported on TiO<sub>2</sub> showed elevated performance compared to that of the photodeposited Au/TiO<sub>2</sub> (2.8 times and 1.9 times, respectively). This trend agrees well with previous observations,<sup>21</sup> as Pt and Pd exhibited larger work functions and therefore a lower Fermi level for improved charge separations compared to that of Au with comparable sizes.<sup>16</sup> Nevertheless, the fine particle sizes of Pt and Pd produced *via* the CVI method might also be a key to promote the photocatalytic H<sub>2</sub> production performance. Alloying Pt with Pd slightly improved the H<sub>2</sub> evolution

performance compared to that of the monometallic counterparts. Furthermore, we found that the microstructure of the metal NPs strongly influence the performance of the photocatalyst. A significant promotional effect was observed for Pd<sub>3</sub>Au<sub>c</sub> and Pt<sub>3</sub>Au<sub>c</sub> supported on TiO<sub>2</sub>, which agreed well with our previous observation on the sol-immobilised metal NPs.<sup>21</sup> Noticeably, an optimum H<sub>2</sub> production rate of ~0.36 mmol·h<sup>-1</sup> that corresponds to a AQE of ~30 % was achieved using the Pd<sub>3</sub>Au<sub>c</sub>/TiO<sub>2</sub>, which was ~2.1 times higher than that of the Pd/TiO<sub>2</sub>.

We have also investigated the photocatalytic oxidation performance of the catalysts by following the CO<sub>2</sub> evolution during the phenol decomposition, as shown in Fig. 5(a). Similar to the H<sub>2</sub> evolution, the CO<sub>2</sub> evolution started as soon as the UV irradiation was commenced. Note that most metal NPs decorated TiO<sub>2</sub> produce CO<sub>2</sub> at roughly constant rates except the Pt/TiO<sub>2</sub>. The CO<sub>2</sub> generation rates followed the order Pt<sub>3</sub>Au<sub>c</sub> > Pd<sub>3</sub>Au<sub>c</sub> ≈ Pd > Pd<sub>1</sub>Pt<sub>1</sub> ≈ Au (photodeposited). The Pt/TiO<sub>2</sub> photocatalyst showed a gradual increase of the CO<sub>2</sub> generation rate as the phenol concentration decreased, indicating it is optimised for working at low phenol concentrations. Since the initial phenol concentration was 400 μM and the total volume was 25 mL for all experiments, a complete decomposition of phenol would correspond to a total amount of 60 μmol of CO<sub>2</sub>.

We have further evaluated the effective phenol decomposition efficiencies (D<sub>e</sub>) and AQE of the photocatalysts using the following equations and shown in Fig. 5(b):

$$D_e = n(\text{CO}_2)/[6n(\text{phenol})] \quad (6)$$

$$\text{AQE} = 6[n(\text{CO}_2)]/n[(\text{incident photons})] \quad (7)$$

where n(CO<sub>2</sub>) and n(phenol) are the numbers of produced CO<sub>2</sub> and the initial phenol molecules, respectively. The n(CO<sub>2</sub>) and n(incident photons) are the numbers of produced CO<sub>2</sub> within the constant CO<sub>2</sub> evolution region and the corresponding numbers of incident photons.

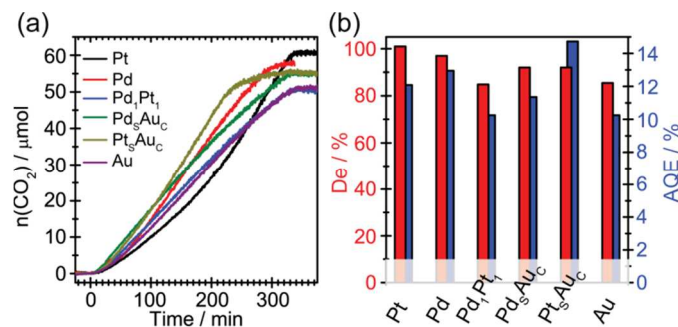


Fig. 5. (a): The CO<sub>2</sub> evolution during photocatalytic phenol decomposition using the as-prepared metal NPs supported on TiO<sub>2</sub> catalyst materials. A 400 μM of phenol solution (25 mL) was used for all measurements thus the initial amount of phenol was 10 μmol. (b): The derived effective decomposition efficiencies (D<sub>e</sub>) of phenol to CO<sub>2</sub> and the apparent quantum efficiencies (AQE) of the metal NPs supported on TiO<sub>2</sub> catalyst materials. All catalysts have a metal loading of 2.5 wt%.

Apparently, complete decomposition of phenol can be realised only using Pt, whereas the rest of NPs variants supported on TiO<sub>2</sub> show incomplete oxidation of phenol. Replacing Pt by Pd slightly increased the AQE but decreased the effective decomposition of phenol as well. Interestingly, alloying Pd with Pt presented negative effects toward both D<sub>e</sub> and AQE. While the core-shell Pt<sub>3</sub>Au<sub>c</sub>/TiO<sub>2</sub> presented the optimum AQE, a slight reduction of D<sub>e</sub> (~90 %) was noticed. Note that the final n(CO<sub>2</sub>) did not exceed the expected amount

(60 μmol), which again supported our assertion that the as-prepared catalysts are ligands free.

## Conclusions

We have presented a chemical vapour impregnation (CVI) method for the deposition of ultra-fine metal NPs co-catalysts on photocatalyst materials. The composition and microstructure of the NPs can be easily adjusted by tuning the precursor composition and deposition sequence without changing the dispersion and particle size distributions. To demonstrate this TiO<sub>2</sub> was modified by monometallic (Pt and Pd), bimetallic alloy (Pt<sub>1</sub>Pd<sub>1</sub>), and core-shell (Pt<sub>3</sub>Au<sub>c</sub> and Pd<sub>3</sub>Au<sub>c</sub>) NPs. Compared to the metal NPs that prepared *via* conventional sol-immobilisation process, the as-deposited metal NPs by the CVI method exhibit surfaces that are free of capping ligands, which required no post-treatment and are immediately ready for photocatalysis applications.

The effect of the composition and microstructure on the photocatalytic performances have been evaluated by hydrogen evolution and phenol decomposition. For H<sub>2</sub> evolution, a significant enhancement of the performance can be achieved by fine tuning of the co-catalyst, and the AQE followed the order Pd<sub>3</sub>Au<sub>c</sub> > Pt<sub>3</sub>Au<sub>c</sub> > Pd<sub>1</sub>Pt<sub>1</sub> > Pt > Pd. For phenol decomposition, adjusting the co-catalyst materials only influenced the photocatalytic performance slightly and the trends observed were more complicated. The Pt/TiO<sub>2</sub> gave a 100 % phenol decomposition, but with a relatively low AQE at high concentrations of phenol. A negative effect on the performance was observed when using the alloy NPs for phenol decomposition. The Pt<sub>3</sub>Au<sub>c</sub>/TiO<sub>2</sub> showed the optimum AQE but a slight reduced D<sub>e</sub> (~90 %) was noticed.

We consider that the CVI approach can be easily applied to the modification of other photocatalyst materials, and their performances can be further improved by fine tuning the physical properties (*i.e.*, loading, identity, structure) of the metal NPs.

## Acknowledgements

We thank the financial support from the iNANO Center through the Danish Strategic Research Council and the Carlsberg Foundation, the Center for Materials Crystallography (Denmark National Research Foundation, DNRF93), and the Chinese Scholarship Council (CSC). We also acknowledge the EPSRC (EP/K014854/1) and NSF for financial support.

## Notes and references

- <sup>a</sup> Interdisciplinary Nanoscience Center (iNANO) and Department of Physics and Astronomy, Aarhus University, Ny Munkegade, DK-8000 Aarhus C, Denmark.
- <sup>b</sup> Cardiff Catalysis Institute, School of Chemistry, Cardiff University, CF10 3AT, Cardiff, UK.
- <sup>c</sup> Department of Chemistry, University of the West Indies, St. Augustine Campus, Trinidad and Tobago.
- <sup>d</sup> Department of Materials Science and Engineering, Lehigh University, 5 East Packer Avenue, 18015-3195, Bethlehem, Pennsylvania, USA.
- <sup>e</sup> Department of Chemistry and Interdisciplinary Nanoscience Center (iNANO), Aarhus University, Langelandsgade 140, DK-8000 Aarhus C, Denmark.
- <sup>f</sup> School of Chemical Engineering and Technology, Harbin Institute of Technology, 150001 Harbin, China.
- <sup>g</sup> The UK Catalysis Hub, Research Complex at Harwell, Rutherford Appleton Laboratory, Oxfordshire, OX11 0FA, UK.
- <sup>†</sup> Electronic Supplementary Information (ESI) available: Additional HAADF-STEM images and XPS spectra. See DOI: 10.1039/b000000x/

1. X. B. Chen, L. Liu, P. Y. Yu and S. S. Mao, *Science*, 2011, **331**, 746.
2. M. R. Hoffmann, S. T. Martin, W. Y. Choi and D. W. Bahnemann, *Chem. Rev.*, 1995, **95**, 69.
3. S. U. M. Khan, M. Al-Shahry and W. B. Ingler, *Science*, 2002, **297**, 2243.
4. A. Fujishima and K. Honda, *Nature*, 1972, **238**, 37.
5. W. Bahnemann, M. Muneer and M. M. Haque, *Catal. Today*, 2007, **124**, 133.
6. K. Sunada, T. Watanabe and K. Hashimoto, *J. Photochem. Photobiol., A*, 2003, **156**, 227.
7. R. L. Ziolli and W. F. Jardim, *J. Photochem. Photobiol., A*, 2002, **147**, 205.
8. A. Fujishima, X. T. Zhang and D. A. Tryk, *Surf. Sci. Rep.*, 2008, **63**, 515.
9. M. A. Henderson, *Surf. Sci. Rep.*, 2011, **66**, 185.
10. J. Pan, G. Liu, G. M. Lu and H. M. Cheng, *Angew. Chem. Int. Ed.*, 2011, **50**, 2133.
11. R. Su, R. Bechstein, J. Kibsgaard, R. T. Vang and F. Besenbacher, *J. Mater. Chem.*, 2012, **22**, 23755.
12. R. Su, R. Bechstein, L. So, R. T. Vang, M. Sillassen, B. Esbjornsson, A. Palmqvist and F. Besenbacher, *J. Phys. Chem. C*, 2011, **115**, 24287.
13. B. Ohtani, O. O. Prieto-Mahaney, D. Li and R. Abe, *J. Photochem. Photobiol., A*, 2010, **216**, 179.
14. K. Maeda, M. Higashi, D. L. Lu, R. Abe and K. Domen, *J. Am. Chem. Soc.*, 2010, **132**, 5858.
15. W. Sun, S. Q. Zhang, C. Wang, Z. X. Liu and Z. Q. Mao, *Catal. Lett.*, 2008, **123**, 282.
16. J. Yang, D. Wang, H. Han and C. Li, *Acc. Chem. Res.*, 2013, **46**, 1900.
17. T. A. Kandiel, R. Dillert and D. W. Bahnemann, *Photochem. Photobiol. Sci.*, 2009, **8**, 683.
18. M. H. Cheng, M. S. Zhu, Y. K. Du and P. Yang, *Int. J. Hydrogen Energ.*, 2013, **38**, 8631.
19. D. Ferrer, A. Torres-Castro, X. Gao, S. Sepulveda-Guzman, U. Ortiz-Mendez and M. Jose-Yacamán, *Nano Lett.*, 2007, **7**, 1701.
20. M. Murdoch, G. I. N. Waterhouse, M. A. Nadeem, J. B. Metson, M. A. Keane, R. F. Howe, J. Llorca and H. Idriss, *Nat. Chem.*, 2011, **3**, 489.
21. R. Su, R. Tiruvalam, A. J. Logsdail, Q. He, C. A. Downing, M. T. Jensen, N. Dimitratos, L. Kesavan, P. P. Wells, R. Bechstein, H. H. Jensen, S. Wendt, C. R. A. Catlow, C. J. Kiely, G. J. Hutchings and F. Besenbacher, *ACS Nano*, 2014, **8**, 3490.
22. A. Takai and P. V. Kamat, *ACS Nano*, 2011, **5**, 7369.
23. H. J. Yan, J. H. Yang, G. J. Ma, G. P. Wu, X. Zong, Z. B. Lei, J. Y. Shi and C. Li, *J. Catal.*, 2009, **266**, 165.
24. F. Y. Wen, J. H. Yang, X. Zong, B. J. Ma, D. G. Wang and C. Li, *J. Catal.*, 2011, **281**, 318.
25. F. Y. Wen, X. L. Wang, L. Huang, G. J. Ma, J. H. Yang and C. Li, *ChemSusChem*, 2012, **5**, 849.
26. J. T. Carneiro, C. C. Yang, J. A. Moma, J. A. Moulijn and G. Mul, *Catal. Lett.*, 2009, **129**, 12.
27. I. Paramasivalm, J. M. Macak and P. Schmuki, *Electrochem. Commun.*, 2008, **10**, 71.
28. A. Orlov, M. S. Chan, D. A. Jefferson, D. Zhou, R. J. Lynch and R. M. Lambert, *Environ. Technol.*, 2006, **27**, 747.
29. R. Su, R. Tiruvalam, Q. He, N. Dimitratos, L. Kesavan, C. Hammond, J. A. Lopez-Sanchez, R. Bechstein, C. J. Kiely, G. J. Hutchings and F. Besenbacher, *ACS Nano*, 2012, **6**, 6284.
30. A. Primo, A. Corma and H. Garcia, *Phys. Chem. Chem. Phys.*, 2011, **13**, 886.
31. K. Mogyorosi, A. Kmetyko, N. Czirbus, G. Vereb, P. Sipos and A. Dombi, *React. Kinet. Catal. L*, 2009, **98**, 215.
32. S. Rawalekar and T. Mokari, *Adv. Energy Mater.*, 2013, **3**, 12.
33. A. J. Logsdail and R. L. Johnston, *RSC Adv.*, 2012, **2**, 5863.
34. H. Bahruji, M. Bowker, P. R. Davies and F. Pedrono, *Appl. Catal., B*, 2011, **107**, 205.
35. N. Dimitratos, J. A. Lopez-Sanchez and G. J. Hutchings, *Chem. Sci.*, 2012, **3**, 20.
36. J. Pritchard, L. Kesavan, M. Piccinini, Q. He, R. Tiruvalam, N. Dimitratos, J. A. Lopez-Sanchez, A. F. Carley, J. K. Edwards, C. J. Kiely and G. J. Hutchings, *Langmuir*, 2010, **26**, 16568.
37. R. C. Tiruvalam, J. C. Pritchard, N. Dimitratos, J. A. Lopez-Sanchez, J. K. Edwards, A. F. Carley, G. J. Hutchings and C. J. Kiely, *Faraday Discuss.*, 2011, 152, 63-86.
38. M. M. Forde, L. Kesavan, M. I. bin Saiman, Q. He, N. Dimitratos, J. A. Lopez-Sanchez, R. L. Jenkins, S. H. Taylor, C. J. Kiely and G. J. Hutchings, *ACS Nano*, 2013, **8**, 957.
39. J. A. Lopez-Sanchez, N. Dimitratos, C. Hammond, G. L. Brett, L. Kesavan, S. White, P. Miedziak, R. Tiruvalam, R. L. Jenkins, A. F. Carley, D. Knight, C. J. Kiely and G. J. Hutchings, *Nat. Chem.*, 2011, **3**, 551.
40. G. R. Bamwenda, S. Tsubota, T. Nakamura and M. Haruta, *J. Photochem. Photobiol., A*, 1995, **89**, 177.
41. T. H. Fleisch and G. J. Mains, *J. Phys. Chem.*, 1986, **90**, 5317.
42. E. Janin, M. Bjorkqvist, T. M. Grehk, M. Gothelid, C. M. Pradier, U. O. Karlsson and A. Rosengren, *Appl. Surf. Sci.*, 1996, **99**, 371.
43. S. Tanuma, C. J. Powell and D. R. Penn, *Surf. Interface Anal.*, 1993, **20**, 77.